Available online at www.sciencedirect.com
ScienceDirect
Renewable Energy 33 (2008) 342–347
RENEWABLE ENERGY
www.elsevier.com/locate/renene

Development of thermoelectric oxides for renewable energy conversion technologies

A. Weidenkaff[a,*], R. Robert[a], M. Aguirre[a], L. Bocher[a], T. Lippert[b], S. Canulescu[b]

[a]*Solid State Chemistry and Catalysis, Empa, Ueberlandstr. 129, CH-8600 Duebendorf, Switzerland*
[b]*Paul Scherrer Institut, Villigen, Switzerland*

Available online 2 July 2007

Abstract

Geothermal and solar heat can be directly converted into electricity by using thermoelectric generators. Perovskite-type metal oxides are potential materials to improve the efficiency of these devices. Cobaltates with *p*-type conductivity and *n*-type manganates are considered for the development of a ceramic thermoelectric converter.

Sintered pellets and thin PLD films with the composition $La_{1-x}Ca_xMO_{3-\delta}$ ($x = 0$, 0.3, 0.4) (M = Co, Mn) were synthesised and characterised concerning their thermoelectric properties in a broad temperature range. It was found that similar to polycrystalline samples the electrical conductivity of $LaCoO_3$ increases significantly with 40% Ca-substitution due to the formation of Co^{4+} ions while the thermopower decreases. The thermopower values of the $La_{0.8}Ca_{0.2}MnO_{3-\delta}$ films have a negative sign, but become large and positive at temperatures of 1000 K.

Keywords: Solar energy; Thermoelectricity; Geothermal energy; Perovskites; Thin films

1. Introduction

With thermoelectric devices, heat can be directly converted into electricity. The use of geothermal or solar heat as energy source for a thermoelectric generator is an attractive and environmentally clean (CO_2-free) proposal to generate electrical power [1, 2]. Thermoelectric converters do not depend on mechanical or chemical conversion processes. Thus, they are emission free during operation, noiseless and extremely durable. The amount of electrical power produced is depending on the thermoelectric conversion efficiency of the device and the heat flux.

The direct conversion of the heat flux into electricity is connected to electron transport phenomena, and the interrelated Seebeck effect. Thermoelectric power is defined as the entropy (or heat) carried by an electron [3].

The direct efficient thermoelectric conversion of solar or geothermal heat into electricity requires the development of *p*- and *n*-type semiconductors with similar materials properties. In general, compounds exhibiting a considerably large Seebeck coefficient S, high electrical conductivity σ, and a small thermal conductivity κ , in summary, a large thermoelectric figure of merit ZT are required.

$$ZT = S^2\sigma T/\kappa. \quad (1)$$

Since these transport properties are interconnected by the Wiedemann–Franz law for most materials, the development of a material breaking this relationship is a scientific challenge. Classic thermoelectric materials suffer from high toxicity, low stability and low efficiency [4], while ceramics have been recently recognised as good thermoelectrics with high stability even at elevated temperatures and low production costs.

Lately large thermopower was discovered in perovskite-type materials making them promising candidates for future thermoelectric applications [5,6]. The thermoelectric effect relies on the fact that the flow of electrons in a solid produces entropy current as well as a charge current. In complex transition metal-oxides the spin of electrons can become an additional source of entropy resulting in the large thermopower in these systems [7].

*Corresponding author.
E-mail address: anke.weidenkaff@empa.ch (A. Weidenkaff).

0960-1481/$ - see front matter © 2007 Elsevier Ltd. All rights reserved.
doi:10.1016/j.renene.2007.05.032

Transition metal-oxides with perovskite structure are potential candidates for thermoelectric devices operating at high temperatures as they can possess large positive as well as large negative thermopower depending on their composition [8–10].

The three parameters defining the thermoelectric figure of merit ZT are in most cases interdependent, i.e. as the thermopower increases so does the resistivity; as the electric conductivity increases so does the heat conductivity. Therefore an optimum charge carrier concentration and mobility has to be defined, which is depending on factors like the substitution level, the spin states of the transition metals, the ligand field, i.e. the crystallographic structure, the valence states of the cations, ionic deficiencies, etc. The heat conductivity can be lowered with suitable substitutions, complex crystal structures or by enhanced boundary scattering in nanostructured materials without changing the electronic transport [11].

For the realisation of cascades of thermoelectric oxide thermocouples to convert the applied temperature gradient of geothermal and/or solar heat exchanger systems into electric power (see Fig. 1), improved thermoelectric materials with *p*-type conductivity as well as compounds with *n*-type conductivity have to be developed. In these devices several *p*- and *n*-legs will be connected electrically in series and thermally in parallel to produce an open circuit voltage of several volts at even low-temperature gradients. A reduction of the size of the thermoelectric elements should further serve to increase the specific power (W/cm^2) of the device due to the increased surface area [12]. For the fabrication of the oxide thermoelectric generator thin film deposition with further structuring procedures are considered.

The $LaCoO_3$ system is a promising thermoelectric material due to its high Seebeck coefficient of 600 μV/K at room temperature. The thermopower of $LaCoO_3$ is positive due to the partial disproportionation $2\ Co^{3+} \leftrightarrow Co^{2+} + Co^{4+}$. Nevertheless the electrical resistivity is rather high (10 Ω cm) which lowers the conversion efficiency. The amount of charge carriers and thus the electrical conductivity and thermoelectric properties in this system can be tuned by suitable Co-site and La-site substitution.

For the *n*-type legs manganates phases are considered and prepared as powders and thin films.

Polycrystalline powder samples as well as thin epitaxial films of the same compositions were produced and characterised to study grain size influences on the transport properties.

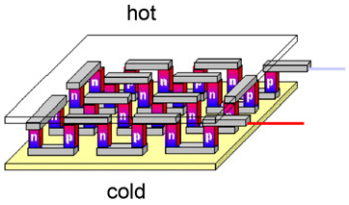

Fig. 1. Cascade of thermoelectric *p*- and *n*-type elements.

2. Experimental

Powders of substituted La-cobaltates and manganates were synthesised with diverse precursor reactions. The precursors were obtained by dissolving the required amount of $La(NO_3)_3 * 6\ H_2O$ (Merck, ⩾97%), $Mn(NO_3)_2 * 6\ H_2O$ (Merck, ⩾99%), $Ca(NO_3)_2 * 6\ H_2O$ (Merck, ⩾97%) and $Co(NO_3)_2 * 6\ H_2O$ (Merck, ⩾97%) in water and mixing them with a chelating agent, e.g. citric acid. These complexes were polymerised in a second step and dried to obtain homogeneous aerogel precursors. Phase purity of the products was confirmed by X-ray diffraction (XRD) data collected on a Siemens D5000 diffractometer equipped with Eulerian cradle using Cu-Kα radiation. X-ray pole figures were measured by rotating the sample around φ-axis and tilting the sample along χ-axis during the measurements with a fixed detector position (2θ). The structure of the samples was further studied by transmission electron microscopy (TEM) using a Philips CM 30. The oxygen content of the powders was determined by the hot gas extraction method using a LECO TC 500. The composition of the films was analysed by the use of Rutherford backscattering spectrometry (RBS) at the PSI/ETH Laboratory for Ion Beam Physics. RBS measurements were performed using a 2 MeV ^4He beam and a silicon surface barrier detector under 165°. The collected RBS data were simulated using the RUMP software [13].

Thin films of $La_{0.6}Ca_{0.4}CoO_3$, $La_{0.7}Ca_{0.3}CoO_3$, $La_{0.7}Ca_{0.3}MnO_3$, $La_{0.6}Ca_{0.4}MnO_3$, and $La_{0.8}Ca_{0.2}MnO_3$ (LCMO) were deposited by PRCLA, using a rotating rod target, which was sintered from powders prepared by the method described above (thermal decomposition of the corresponding polymeric precursors).

The target material is located at a distance of 4.5 cm from the substrate. A KrF excimer laser ($\lambda = 248$ nm) with a pulse duration of 17 ns was used as the irradiation source. The target was ablated with a laser fluence of 7.6 J cm^{-2} at a repetition rate of 10 Hz with 20 000–30 000 pulses for each film.

The lattice mismatch of the heteroepitaxial films is varied by using different substrate materials of $10 \times 10 \times 0.5\ mm^3$ size, i.e. MgO with $a = 0.421$ nm, $SrTiO_3$ (STO) with $a = 0.3905$ nm or $LaAlO_3$ (LAO) with $a = 0.3788$ nm. The substrates were rotated during the deposition to obtain uniform film thickness and heated to a typical temperature of 650 °C. The films were cooled with a vented chamber and a cooling rate of ≈40 °C/min. The film thickness and surface roughness were measured with a profilometer (Dektak 8000).

The transport property measurements were performed on bar shaped pressed-sintered pellets with general dimensions of 1.65 mm × 5 mm × 1 mm as well as on thin films. The electrical conductivity and Seebeck coefficient were measured in air simultaneously as a function of temperature

from 340 to 1273 K using a RZ2001i measurement system from Ozawa Science, Japan. The electrical conductivity was determined using a four-point probe method. Two electrical contacts were positioned at both ends of the sample and the two others contacts were on the sample body. Circular pellets (10 mm diameter) of the same composition were used for thermal conductivity measurements by the laser flash method using a Netzsch LFA-457 apparatus from 300 to 1020 K in argon atmosphere.

3. Results

A series of *A*- and *B*-site substituted lanthanum cobaltate and manganate compounds with various compositions and perovskite structure have been successfully synthesised by a polymeric precursor method [14]. The fine black powders obtained at $T = 873$ K reveal a uniform particle size of approximately 70 nm in diameter. After further annealing to 1273 K, the sintering processes lead to an increase of particle size by a factor of 8. All samples are single phase and crystallise in rhombohedral crystal structure.

These materials were laser ablated and deposited in a PRCLA-process [15–17]. The resulting films of 200–300 nm thickness are generally black and highly reflecting. Rutherford back scattering (RBS) analysis of the elemental film composition confirms that the ablation is congruent.

Samples with the composition $La_{0.8}Ca_{0.2}MnO_3$ and $La_{0.6}Ca_4CoO_3$ were successfully grown in an epitaxial way on LAO and MgO single crystalline substrates.

3.1. Manganates

$La_{1-x}Ca_xMnO_3$ ($x = 0.2, 0.3, 0.4$) were grown on MgO and LAO substrates. The X-ray diffractogram of the $La_{0.8}Ca_{0.2}MnO_3$ film grown on an $LaAlO_3$ with 20000 pulses reveals only (1 0 0), (200) and (300) pseudocubic reflexes of the perovskite-phase and substrate (see Fig. 2).

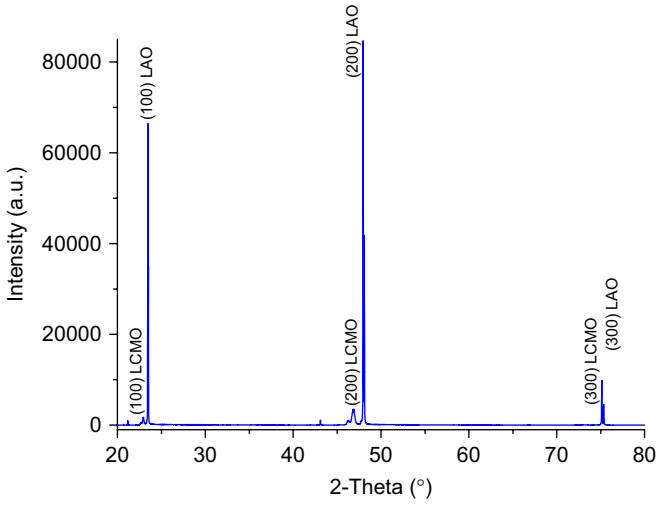

Fig. 2. XRD pattern of the oriented $La_{0.8}Ca_{0.2}MnO_3$ (LCMO) thin solid film on LAO.

This result confirms that the 480 nm thin film was grown epitaxially and has a slightly distorted pseudocubic crystallographic structure [18].

The electrical resistivity of all LCMO films decreases with increasing temperature (see Fig. 3b), representing a semiconducting-like behaviour ($d\rho/dT<0$). The Seebeck coefficient has negative values up to 750 K. At higher temperature it becomes positive and reaches very large values of up to 120 μV/K at 1000 K.

3.2. Cobaltates

Lanthanum cobaltate thin films with 40% calcium content were grown in a similar procedure [19]. The deposition after 20 000 laser pulses reveals dense films of 200 nm thickness. The high resolution TEM image in cross sectional view, shown in Fig. 4 represents the sharp interface between the MgO substrate (lower part) and a dense highly crystalline $La_{0.6}Ca_{0.4}CoO_3$ film (upper part). The stress during the initial deposition process — caused by the impinging of activated species on the substrate surface and the 10% lattice misfit between MgO and $La_{0.7}Ca_3CoO_3$ — is relaxed into the substrate and the film. The electron diffraction (ED) pattern reveals a cubic cell with $a = 0.380$ nm which is comparable to values of the stress free $La_{0.7}Ca_{0.3}CoO_3$ powder ($a = 0.3790$ nm) and show furthermore that the $(0\,0\,2)_{LCC}$ planes are oriented parallel to the $(0\,0\,2)_{MgO}$ planes.

Fig. 5 shows the (1 1 1) pole figure of the $La_{1-x}Ca_xCoO_3$ film at a 2θ angle at 42.97°. In the figure four maxima at $\chi = 54°$ are visible, indicative of the epitaxial single-crystalline cubic domains of the orientated film.

The Seebeck coefficient of the cobaltate samples is positive in the whole temperature range from 300 to 1273 K indicating predominant positive charge carriers, while the Seebeck coefficient of the manganates samples changes the sign with temperature.

The substitution of Ca for La in the 3D-compound decreases the electrical resistivity to values of 0.1 Ω cm (films) and 0.01 Ω cm (pressed powders) for $x = 0.4$ at room temperature. This considerable decrease of the electrical resistivity is associated with an increase of Co^{4+} ions and thus the number of holes in the mixed valance band. The Co^{4+} formation is induced through substitution of La^{3+} by Ca^{2+}. The value of the thermopower of the Ca-substituted $LaCoO_3$ is $\approx 70\,\mu V K^{-1}$ at 300K. The power factor has a value of 4.9×10^{-6} W/K^2 m at room temperature. At elevated temperature these values change in significantly (see Fig. 6 and Fig. 7). The resistivity of the thin films decreases to values of a few m Ω cm, leading to a simultaneous decrease of the thermopower at high temperature.

The polycrystalline reference samples on the other hand show very low thermopower at higher temperature and metallic conductivity.

The thermal property measurements (not shown here) reveal similar values for the perovskite-type cobaltates and

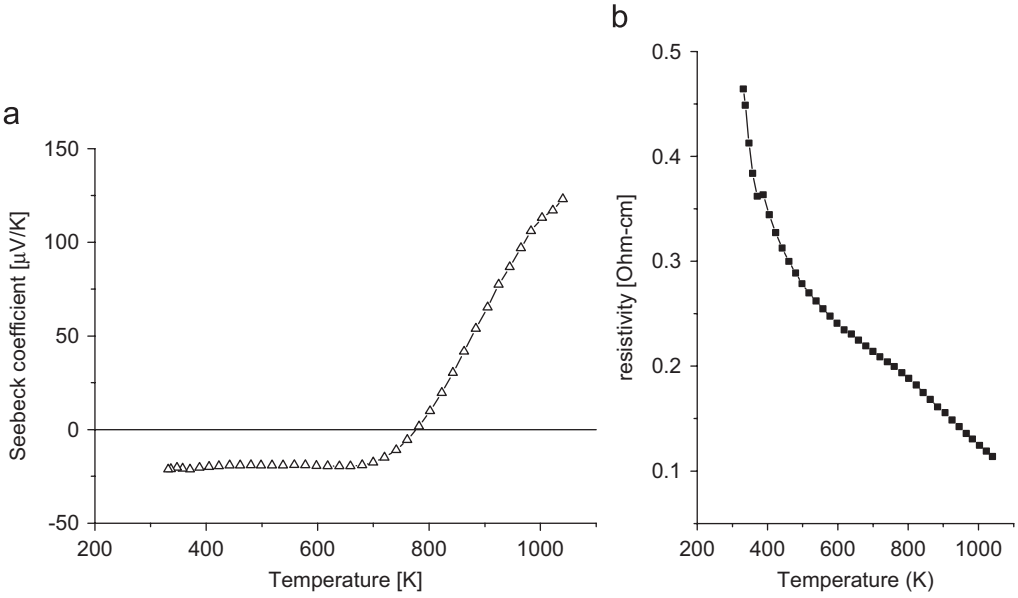

Fig. 3. Thermopower (a) and resistivity (b) in the temperature range $300\,K < T < 1200\,K$ of the LCMO thin film.

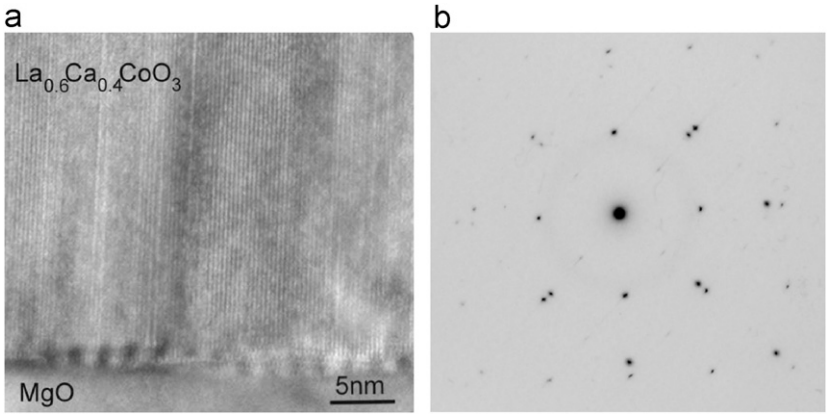

Fig. 4. HRTEM image of (a) the $La_{0.6}Ca_{0.4}CoO_3$ film/MgO interphase and (b) electron diffraction of the $La_{0.6}Ca_{0.4}CoO_3$ film on MgO(0 0 1).

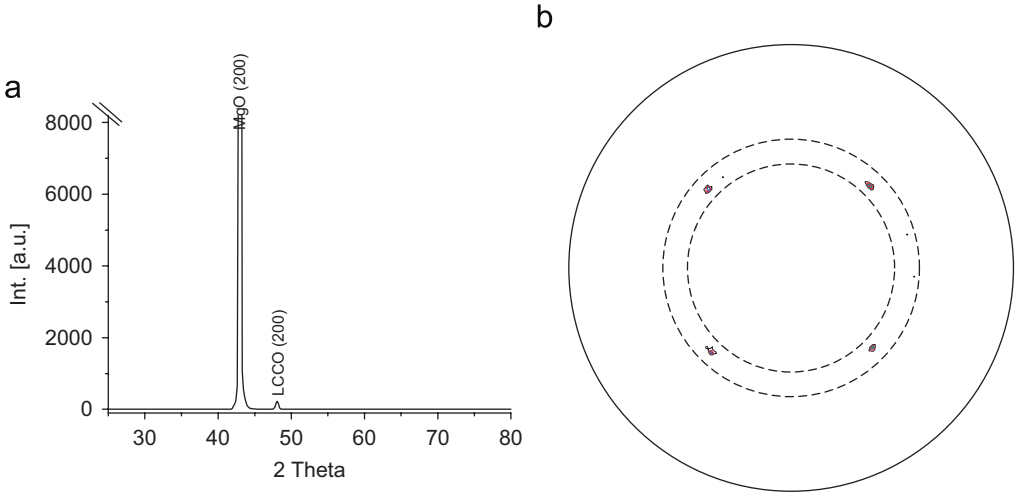

Fig. 5. XRD pattern in logarithmic scale (a) and 111 pole figure (b) of the $La_{0,6}Ca_{0,4}CoO_3$ (LCCO) film on MgO.

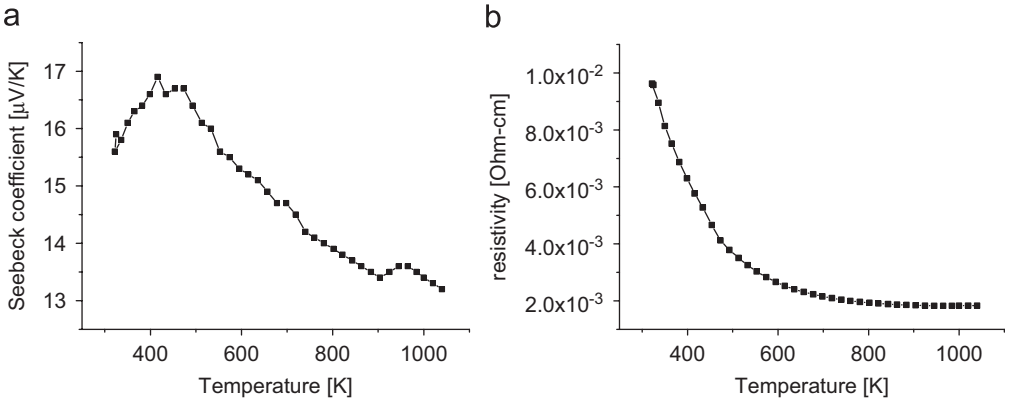

Fig. 6. Temperature dependence of the thermopower (a) and resistivity (b) of a 200 nm $La_{0.6}Ca_{0.4}CoO_3$ film.

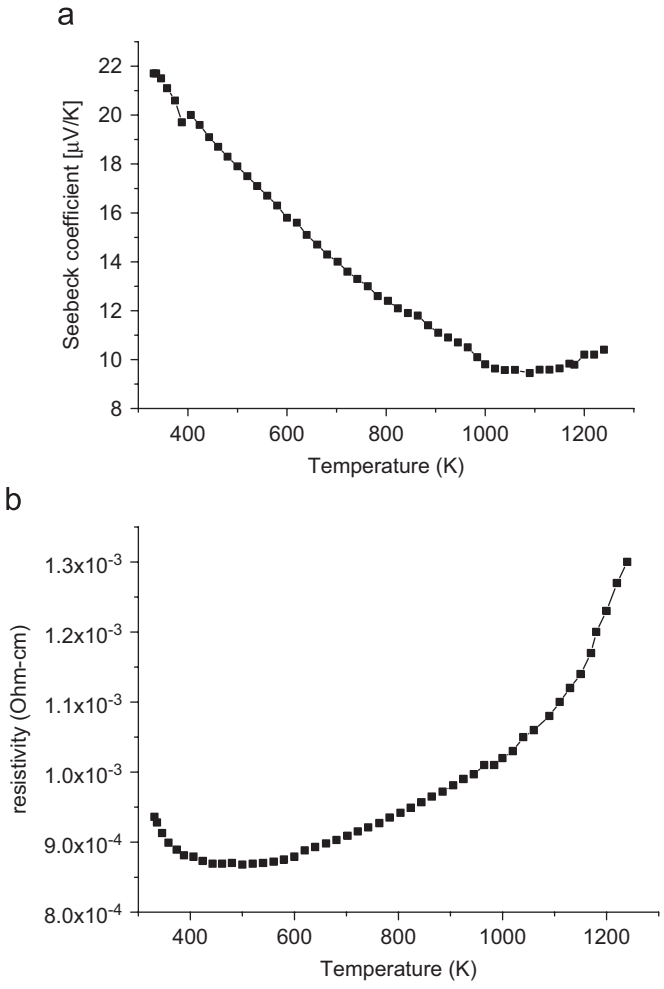

Fig. 7. Temperature dependence of the thermopower (a) and resistivity (b) of polycrystalline $La_{0.6}Ca_{0.4}CoO_3$ pressed powders.

manganates in the whole temperature range from 300 to 1020 K. The measured total thermal conductivity values of the cobaltates vary from 0.5–1.8 W/m K while the manganates samples show thermal conductivities between 1.0 W/m K and 1.5 W/m K depending strongly on the particle size (see also [20]). These low values result in figure of merit (ZT) values of $ZT < 0.2$.

5. Conclusions

Thin epitaxial films and powders of lanthanum calcium cobaltates and manganates with perovskite structure were successfully synthesised and characterised. The electrical conductivity, the Seebeck coefficient and the thermal conductivity were measured in a broad temperature range. The studied perovskite-type oxides are showing a large potential for thermoelectric applications, as the thermopower relies on the tuneable itinerant electrons. The sign and the absolute value of the Seebeck coefficient can be changed with hole or electron doping, i.e. aliovalent cation substitutions.

The electrical resistivity of $LaCoO_3$ decreases significantly with 40% Ca-substitution due to the formation of Co^{4+} ions while the thermopower decreases.

The sign of the thermopower values of the lanthanum calcium manganates samples is negative at low temperatures and becomes large and positive at high temperatures.

Acknowledgements

The authors thank M. Montenegro for the preparation of the cobaltate films and the Swiss Federal Office of Energy for financial support.

References

[1] Rowe DM. Renewable Energy 1999;16:1251–6.
[2] Scherrer H, Vikhor L, Lenoir B, Dauscher A, Poinas P. J. Power Sources 2003;115:141–8.
[3] Kittel C. Solid state physics. New York: Wiley-VCH; 2004.
[4] Bandhari CM, Rowe DM. CRC Handbook of thermoelectrics. Boca Raton: CRC Press; 1995.
[5] Terasaki I, Sasago Y, Uchinokura K. Phys. Rev. B 1997;56:R12685.
[6] Maignan A, Wang LB, Hebert S, Pelloquin D, Raveau B. Chem. of Mater. 2001;14:1231–5.
[7] Wang Y, Rogado NS, Cava RJ, Ong NP. Nature 2003;423:425–8.
[8] Maignan A, Hebert S, Pi L, Pelloquin D, Martin C, Michel C, Hervieu M, Raveau B. Cryst. Eng. 2002;5:365–82.

[9] Fresard R, Hebert S, Maignan A, Pi L, Hejtmanek J. Phys Lett A 2002;303:223–8.
[10] Pollert E, Hejtmanek J, Jirak Z, Knizek K, Marysko M, Doumerc JP, Grenier JC, Etourneau J. J Solid State Chem 2004; 177:4564–8.
[11] Robert R, Romer S, Hebert S, Maignan A, Reller A, Weidenkaff A. Proceedings of the second European conference on thermoelectrics, 2004 p. 194–197.
[12] Matsubara I, Funahashi R, Takeuchi T, Sodeoka S, Shimizu T, Ueno K. Appl Phys Lett 2001;78:3627–9.
[13] Doolittle LR. Nucl Instrum. Methods Phys. Res. Sect. B 1985; 9:344–51.
[14] Weidenkaff A. Adv Eng Mater 2004;6:709–14.
[15] Montenegro MJ, Lippert T, Müller S, Weidenkaff A, Willmott PR, Wokaun A. Appl Surf Sci 2002;198:505–11.
[16] Montenegro MJ, Lippert T, Müller S, Weidenkaff A, Willmott PR, Wokaun A. Phys Chem Chem Phys 2001;4:2799–805.
[17] Canulescu S, Lippert T, Wokaun A, Robert R, Logvinovich D, Weidenkaff A. Prog Solid State Chem, in press.
[18] Canulescu S, Lippert T, Grimmer H, Wokaun A, Robert R, Logvinovich D, Döbeli M, Weidenkaff A. Appl Surf Sci 2006, in press.
[19] Weidenkaff A, Diecker C, Lippert T, Montenegro MJ. Thin Solid Films 2004;453:406–10.
[20] Bocher L, Robert R, Aguirre MH, Schlapbach L. Proceedings of the fourth European conference on thermoelectrics, 2006.